15 October 2000

ELSEVIER

Optics Communications 184 (2000) 493–505

OPTICS COMMUNICATIONS

www.elsevier.com/locate/optcom

Nonlinear analysis of pattern formation in singly resonant second-harmonic generation

P. Lodahl [a,*], M. Saffman [b]

[a] *Department of Optics and Fluid Dynamics, Risø National Laboratory, P.O. Box 49, DK-4000 Roskilde, Denmark*
[b] *Department of Physics, University of Wisconsin, Madison, WI 53706, USA*

Received 7 March 2000; received in revised form 18 August 2000; accepted 31 August 2000

Abstract

A weakly nonlinear multiple-scales analysis is performed for singly resonant second-harmonic generation. Coupled amplitude equations are derived that describe pattern formation above the transverse instability threshold. The amplitude equations explain the absence of roll patterns and are in good agreement with numerical results. © 2000 Elsevier Science B.V. All rights reserved.

PACS: 42.65.Sf; 42.65.Ky
Keywords: Nonlinear optics; Pattern formation

1. Introduction

Substantial efforts have been devoted to investigations of mechanisms behind instabilities and pattern formation in nonlinear systems. Pattern formation may occur when the homogeneous ground state solutions of a nonlinear system destabilize due to strong driving. The instability threshold and spatio-temporal scales are easily derived through a linear stability analysis of the ground state solutions. Detailed knowledge of the pattern formation dynamics above instability threshold is more complicated to access. While numerical simulations can be used to find the nonlinear patterns it is important to have analytical results for comparison. For this purpose a multiple-scales analysis is useful [1,2]. It utilizes a perturbative expansion above instability threshold taking into account the nature of the instability and the type of modulated solution under investigation. The resulting amplitude equations can be used to derive expressions for the pattern amplitudes valid to lowest order in the expansion parameter ϵ. Furthermore, they can also be used to obtain important analytical information about the mutual stability of the various patterns in a nonlinear system.

In optics different types of nonlinearities can be accessed depending on the experimental configuration under investigation. $\chi^{(2)}$ cavity enhanced processes turn out to be interesting pattern forming systems as was first proposed by Oppo et al. [3,4] in their work on the optical parametric oscillator (OPO). The tendency

* Corresponding author. Fax: +45-4677-4588.
E-mail address: peter.lodahl@risoe.dk (P. Lodahl).

0030-4018/00/$ - see front matter © 2000 Elsevier Science B.V. All rights reserved.
PII: S0030-4018(00)00971-8

for the degenerate, detuned OPO to exhibit roll patterns was explored, and explained to be due to momentum conservation in the parametric conversion process. Furthermore, good agreement between numerical simulations and a multiple-scales analysis was obtained. Further investigations of the degenerate OPO were performed in Ref. [5] including the formation of hexagons and identification of secondary instabilities of rolls of both the Eckhaus and zig-zag type. For the nondegenerate OPO a detailed multiple-scale derivation was given by Longhi [6]. He explained analytically the absence of roll patterns and the presence of off-axis traveling wave solutions. A similar result has been obtained for the Maxwell–Bloch equations describing lasers [7–9]. Pattern formation in doubly resonant second-harmonic generation (SHG) was first treated in Ref. [10]. Here the linear stability analysis was supplemented by numerical investigations to demonstrate the existence of stationary hexagons and time-oscillating rolls. Moreover, nondegenerate type-II SHG has been studied [11] including a multiple-scale analysis of the numerically observed square patterns [12], in addition to the more complicated quasi-patterns [13,14].

In this paper we consider the process of phase-mismatched singly resonant SHG (SRSHG), where the fundamental field is resonated in a cavity, while the second harmonic escapes the cavity freely. Pattern formation in this configuration was first described in Ref. [15]. It was pointed out to be important to consider the possibility for the generated second harmonic to pump a competing parametric process. This complicated the pattern analysis substantially, leading to three coupled equations. Exact analytical solutions above threshold for the parametric process in doubly resonant SHG have been found both without [16] and with [17] inclusion of diffraction. For simplicity we restrict attention here to the case where the parametric process is not excited. Hence, the analysis only applies to the situation where the pattern forming SHG instability is below the parametric threshold.

The purpose of this paper is to derive amplitude equations for the patterns found in SRSHG. In Section 2 we derive coupled Newell–Whitehead–Segel amplitude equations that describe roll, square and hexagonal patterns. The amplitude equations are solved in Section 3 and the results are compared with numerics. Furthermore, the mutual stability of rolls and squares is investigated, and the nonexistence of roll patterns explained.

2. Derivation of the amplitude equations

In this section we outline the derivation of amplitude equations for roll, square, and hexagonal patterns. The analysis starts from the scaled mean-field equation for the resonant fundamental field amplitude A in SRSHG given by

$$\frac{\partial A}{\partial t} = (-1 + \mathrm{i}\Delta)A + f(\xi)|A|^2 A + \mathrm{i}\nabla_\perp^2 A + E. \tag{1}$$

The detailed derivation and description of this equation can be found in Ref. [15]. It describes the spatio-temporal evolution of the intracavity fundamental field A. The fundamental loss term has been scaled to unity, while Δ is the cavity detuning, and E is the amplitude of the fundamental pump field incident on the cavity. We define the phase-mismatch parameter $\xi = (2k_1 - k_2)L$, where k_1, k_2 are the wave numbers of the fundamental and second harmonic respectively, and L is the length of the $\chi^{(2)}$ nonlinear crystal. The nonlinear term is effectively cubic in the singly resonant configuration, since the second-harmonic field can be eliminated from the equation for the fundamental. The complex nonlinear coefficient is given by the function

$$f(\xi) = \frac{2\mathrm{i}}{\xi} + \frac{\mathrm{e}^{-2\mathrm{i}\xi} - 1}{\xi^2}. \tag{2}$$

Eq. (1) is of the same functional form as the equation for a driven cavity containing a Kerr medium or far detuned two-level atoms [18–21]. Thus, it is worth emphasizing that the derivation of amplitude equations presented in the following also applies to these cases. In general the function $f(\xi)$ has a nonvanishing real part that gives rise to an absorptive nonlinear term. However, for $\xi = \pi m$ where m is an integer, the nonlinearity is seen to be purely dispersive or of the Kerr type. Derivations of amplitude equations for the Kerr limit can be found in Refs. [22,23].

The linear stability analysis which is a prerequisite for the multiple-scale derivation was presented in Ref. [15]. The homogeneous solution A_0 destabilizes with respect to transverse perturbations above a threshold amplitude A_t of magnitude

$$|A_t| = \frac{1}{\sqrt{2f_r(\xi) + |f(\xi)|}}. \tag{3}$$

The corresponding critical transverse instability wave number is

$$k_c = \sqrt{\Delta + \Delta^{(NL)}}, \tag{4}$$

with the nonlinear phase shift $\Delta^{(NL)} = 2f_i(\xi)|A_t|^2$. Here subscripts r and i indicate real and imaginary parts respectively. Fig. 1 shows the parameter regions where the transverse instability exists. A general requirement is $|\xi| \geqslant 1.65$ with further restrictions depending on Δ.

In the following we will only consider the case where a single stable homogeneous solution A_0 exists, i.e. the regions with bistable behavior are discarded. Numerical simulations reveal that localized states are generic in the bistability region but will not be discussed further here. Fig. 2 shows the values of ξ and Δ where the bistability exists. The boundaries are determined from the conditions

$$\Delta = \tan[\pm\pi/6 - \arg(f(\xi))], \tag{5a}$$

$$f_r(\xi) > \Delta f_i(\xi), \tag{5b}$$

where the $\pm$ sign corresponds to ξ positive (negative).

For the multiple-scales analysis it is convenient to subtract the homogeneous part of the amplitude and introduce the new variable $B = A - A_0$. With $\mathbf{v} = (B, B^*)^T$, Eq. (1) can formally be written as $\partial_t \mathbf{v} = \hat{\mathbf{L}}\mathbf{v} + \mathbf{N}$ where

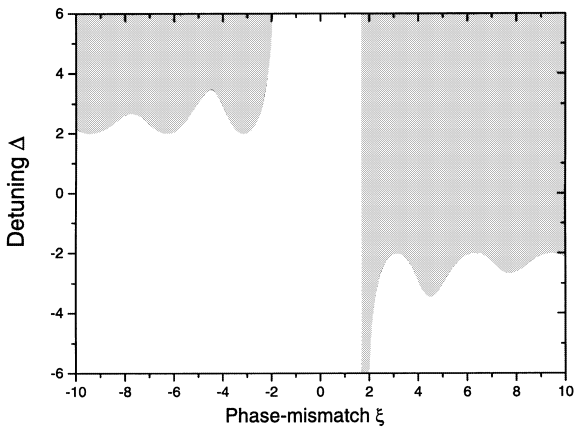

Fig. 1. The shaded areas show the parameter regions where the transverse instability exists.

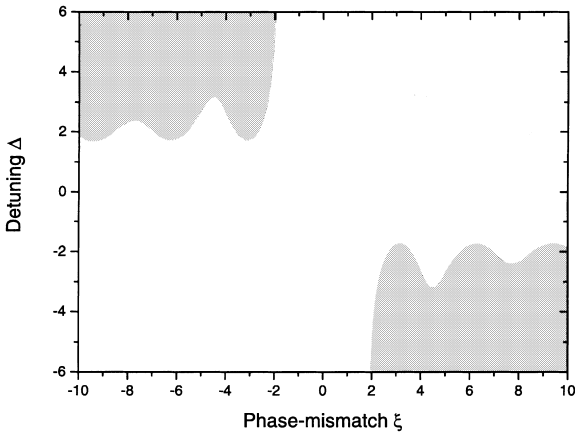

Fig. 2. Shaded areas indicate the bistability regions.

$$\hat{\mathbf{L}} = \begin{bmatrix} -1 + \mathrm{i}\Delta + 2f|A_0|^2 + \mathrm{i}\nabla_\perp^2 & fA_0^2 \\ f^*\left(A_0^*\right)^2 & -1 - \mathrm{i}\Delta + 2f^*|A_0|^2 - \mathrm{i}\nabla_\perp^2 \end{bmatrix}, \tag{6a}$$

$$\mathbf{N} = \begin{pmatrix} 2fA_0|B|^2 + fA_0^*B^2 + f|B|^2B \\ 2f^*A_0^*|B|^2 + f^*A_0B^{*2} + f^*|B|^2B^* \end{pmatrix}, \tag{6b}$$

and the argument of $f(\xi)$ has been dropped for brevity. An expansion parameter ϵ is defined that measures the distance above the instability threshold: $\epsilon^2 = |A_0|/|A_\mathrm{t}| - 1$. It is chosen in order to achieve positive growth rates within a band of wave numbers around k_c of width $\Delta k \sim \epsilon$. We note at this point that with this definition of ϵ subcritical behavior cannot be described since this would lead to an imaginary value of ϵ.

The solution $\mathbf{v}$ is expanded perturbatively in ϵ according to

$$\mathbf{v} = \epsilon\begin{pmatrix} B^{(1)} \\ B^{(1)^*} \end{pmatrix} + \epsilon^2\begin{pmatrix} B^{(2)} \\ B^{(2)^*} \end{pmatrix} + \epsilon^3\begin{pmatrix} B^{(3)} \\ B^{(3)^*} \end{pmatrix}. \tag{7}$$

In the present paper we restrict the discussion to the case of atmost three different critical wave vector components $\mathbf{k}_1$, $\mathbf{k}_2$ and $\mathbf{k}_3$, which includes roll, square and hexagonal patterns. Three different coordinate systems (x_j, y_j), $j = 1, 2, 3$ are introduced rotated by angles θ_{ij} with respect to each other and with the x-axes along the critical wave vectors $\mathbf{k}_j$ that constitute the axes with fast variation. The corresponding slowly varying variables are defined as $T_1 = \epsilon t$, $T_2 = \epsilon^2 t$, $X_j = \epsilon x_j$, $Y_j = \epsilon^{1/2} y_j$, $j = 1, 2, 3$, where small and capital letters denote fast and slow variables, respectively. The asymmetric scaling of x and y coordinates is introduced to have the lowest order slow contributions from perpendicular directions to the same order in ϵ [1].

Due to the invariance of the Laplacian under rotations it can be expanded in any of the coordinate systems and we obtain

$$\nabla_\perp^2 = \nabla_{\perp,0}^2 + \epsilon(\partial_{Y_j}^2 + 2\partial_{x_j}\partial_{X_j}) + \epsilon^2\partial_{X_j}^2, \tag{8}$$

where $\nabla_{\perp,0}^2 = \partial_{x_j}^2 + \partial_{y_j}^2$ is the transverse Laplacian of the rapidly varying variables. Since the instability is stationary the time operator is expanded only in slow variables

$$\partial_t = \epsilon\partial_{T_1} + \epsilon^2\partial_{T_2}. \tag{9}$$

Hence, the operator $\hat{\mathbf{L}}$ and vector $\mathbf{N}$ can be expanded according to

$$\hat{\mathbf{L}} = \hat{\mathbf{L}}_0 + \epsilon\,\hat{\mathbf{L}}_1 + \epsilon^2\,\hat{\mathbf{L}}_2, \tag{10a}$$

$$\mathbf{N} = \epsilon^2\mathbf{N}_2 + \epsilon^3\mathbf{N}_3, \tag{10b}$$

with the components

$$\hat{\mathbf{L}}_0 = \begin{bmatrix} -1 + \mathrm{i}\Delta + 2f|A_\mathrm{t}|^2 + \mathrm{i}\nabla^2_{\perp,0} & fA_\mathrm{t}^2 \\ f^*A_\mathrm{t}^{*2} & -1 - \mathrm{i}\Delta + 2f^*|A_\mathrm{t}|^2 - \mathrm{i}\nabla^2_{\perp,0} \end{bmatrix}, \tag{11a}$$

$$\hat{\mathbf{L}}_1 = \begin{bmatrix} \mathrm{i}\left(\partial^2_{Y_j} + 2\partial_{x_j}\partial_{X_j}\right) & 0 \\ 0 & -\mathrm{i}\left(\partial^2_{Y_j} + 2\partial_{x_j}\partial_{X_j}\right) \end{bmatrix}, \tag{11b}$$

$$\hat{\mathbf{L}}_2 = \begin{bmatrix} 4f|A_\mathrm{t}|^2 + \mathrm{i}\partial^2_{X_j} & 2\chi f A_\mathrm{t}^2 \\ 2\chi^* f^* A_\mathrm{t}^{*2} & 4f^*|A_\mathrm{t}|^2 - \mathrm{i}\partial^2_{X_j} \end{bmatrix}, \tag{11c}$$

$$\mathbf{N}_2 = \begin{pmatrix} 2fA_\mathrm{t}|B^{(1)}|^2 + fA_\mathrm{t}^*B^{(1)^2} \\ 2f^*A_\mathrm{t}^*|B^{(1)}|^2 + f^*A_\mathrm{t}\left(B^{(1)^*}\right)^2 \end{pmatrix}, \tag{12a}$$

$$\mathbf{N}_3 = \begin{pmatrix} 2fA_\mathrm{t}\left(B^{(1)}B^{(2)^*} + B^{(2)}B^{(1)^*}\right) + 2fA_\mathrm{t}^*B^{(1)}B^{(2)} + f|B^{(1)}|^2B^{(1)} \\ 2f^*A_\mathrm{t}^*\left(B^{(1)}B^{(2)^*} + B^{(2)}B^{(1)^*}\right) + 2f^*A_\mathrm{t}B^{(1)^*}B^{(2)^*} + f^*|B^{(1)}|^2B^{(1)^*} \end{pmatrix}. \tag{12b}$$

The phase of A_0 changes above threshold and implies inclusion of the coefficient χ, through $A_0 = A_\mathrm{t}(1+\chi\epsilon^2)$. This implies $|A_0|^2 = |A_\mathrm{t}|^2(1+2\chi_\mathrm{r}\epsilon^2)$ and accordingly $\chi_\mathrm{r} = 1$. It turns out that only the real part of χ is needed in the following. Collecting orders of ϵ gives the set of equations

$$\hat{\mathbf{L}}_0\mathbf{v}^{(1)} = \mathbf{0}, \tag{13a}$$

$$\hat{\mathbf{L}}_0\mathbf{v}^{(2)} = \partial_{T_1}\mathbf{v}^{(1)} - \hat{\mathbf{L}}_1\mathbf{v}^{(1)} - \mathbf{N}_2, \tag{13b}$$

$$\hat{\mathbf{L}}_0\mathbf{v}^{(3)} = \partial_{T_1}\mathbf{v}^{(2)} - \hat{\mathbf{L}}_1\mathbf{v}^{(2)} + \partial_{T_2}\mathbf{v}^{(1)} - \hat{\mathbf{L}}_2\mathbf{v}^{(1)} - \mathbf{N}_3. \tag{13c}$$

A solution of Eq. (13a) of the following form is investigated

$$B^{(1)} = \sum_{j=1}^{N}[\alpha_j(X_j, Y_j, T_1, T_2)\mathrm{e}^{\mathrm{i}k_\mathrm{c}x_j} + \alpha_j^*(X_j, Y_j, T_1, T_2)\mathrm{e}^{\mathrm{i}\phi}\mathrm{e}^{-\mathrm{i}k_\mathrm{c}x_j}], \tag{14}$$

which is a superposition of N rolls. In this paper we restrict to atmost $N = 3$. The phase ϕ is given by

$$\mathrm{e}^{\mathrm{i}\phi} = \frac{fA_\mathrm{t}^2}{1 - 2f_\mathrm{r}|A_\mathrm{t}|^2}. \tag{15}$$

Details in the derivation of the amplitude equations determining the slowly varying amplitudes α_j can be found in Appendix A. In the case of atmost two critical wave vectors they are given by

$$\partial_t\alpha_1 = \Gamma_1\left(\mathrm{i}\partial^2_{y_1} - 2k_\mathrm{c}\partial_{x_1}\right)^2\alpha_1 + 2\epsilon^2\alpha_1 + \epsilon^2\left(\Gamma_2|\alpha_1|^2 + \Gamma_3|\alpha_2|^2\right)\alpha_1, \tag{16a}$$

$$\partial_t\alpha_2 = \Gamma_1\left(\mathrm{i}\partial^2_{y_2} - 2k_\mathrm{c}\partial_{x_2}\right)^2\alpha_2 + 2\epsilon^2\alpha_2 + \epsilon^2\left(\Gamma_3|\alpha_1|^2 + \Gamma_2|\alpha_2|^2\right)\alpha_2, \tag{16b}$$

that can be used to describe roll patterns ($\alpha_2 = 0$) and square patterns ($\alpha_1 = \alpha_2$, $\theta = \pi/2$), as discussed in Section 3. They are of the Newell–Whitehead–Segel form [24,25] and are generic for the transverse instability described here [1]. The form of the equations reflects the symmetry of the pattern-forming instability while the detailed dependence on the physical system under investigation is contained in the coefficients Γ_j that are specified in the appendix.

The analysis can also be extended to the case of three critical wave vectors in order to describe hexagons. This particular case corresponds to the situation where $\theta_{12} = \theta_{23} = \pi/3$, $\theta_{13} = 2\pi/3$. In this case resonant coupling between critical wave vectors leads to the appearance of quadratic nonlinear terms in the amplitude equations that take the form

$$\partial_t \alpha_1 = \Gamma_1 \left(\mathrm{i}\partial_{y_1}^2 - 2k_c \partial_{x_1} \right)^2 \alpha_1 + 2\epsilon^2 \alpha_1 + \tfrac{1}{2}\epsilon \mathrm{e}^{\mathrm{i}\phi/2} \Gamma_4 \alpha_2 \alpha_3^* + \epsilon^2 \left[\Gamma_2 |\alpha_1|^2 + \Gamma_5 \left(|\alpha_2|^2 + |\alpha_3|^2 \right) \right] \alpha_1, \tag{17a}$$

$$\partial_t \alpha_2 = \Gamma_1 \left(\mathrm{i}\partial_{y_2}^2 - 2k_c \partial_{x_2} \right)^2 \alpha_2 + 2\epsilon^2 \alpha_2 + \tfrac{1}{2}\epsilon \mathrm{e}^{-\mathrm{i}\phi/2} \Gamma_4 \alpha_1 \alpha_3 + \epsilon^2 \left[\Gamma_2 |\alpha_2|^2 + \Gamma_5 \left(|\alpha_1|^2 + |\alpha_3|^2 \right) \right] \alpha_2, \tag{17b}$$

$$\partial_t \alpha_3 = \Gamma_1 \left(\mathrm{i}\partial_{y_3}^2 - 2k_c \partial_{x_3} \right)^2 \alpha_3 + 2\epsilon^2 \alpha_3 + \tfrac{1}{2}\epsilon \mathrm{e}^{\mathrm{i}\phi/2} \Gamma_4 \alpha_1^* \alpha_2 + \epsilon^2 \left[\Gamma_2 |\alpha_3|^2 + \Gamma_5 \left(|\alpha_1|^2 + |\alpha_2|^2 \right) \right] \alpha_3, \tag{17c}$$

with Γ_4 and Γ_5 given in Appendix A.

3. Solutions of the amplitude equations

In this section the amplitude equations are compared with numerical solutions of Eq. (1). In Section 3.1 homogeneous solutions of the amplitude equations are found that describe rolls, squares and hexagons, and the pattern amplitudes are directly compared with numerical results. In Section 3.2 the stability of patterns is investigated and it is shown that rolls are unstable in the 2D geometry.

3.1. Comparison of analytical and numerical results

The advantage of the amplitude equations compared to the original equation (1) is that they are much simpler to solve. Hence, the amplitudes of the pattern solution excited above threshold are obtained as stationary solutions. Rolls and squares can be obtained by substituting $\alpha_1 = \alpha_R$, $\alpha_2 = 0$ and $\alpha_1 = \alpha_2 = \alpha_S$, respectively in Eqs. (16a) and (16b)

$$\alpha_R^2 = -\frac{2}{\Gamma_2}, \tag{18a}$$

$$\alpha_S^2 = -\frac{2}{\Gamma_2 + \Gamma_3 \ (\theta = \pi/2)}, \tag{18b}$$

where the amplitudes have been chosen real since the phase only corresponds to an arbitrary shift of the pattern. In contrast, hexagons only exist with certain phase relations fulfilled. Substituting $\alpha_j = \alpha_H \exp(\mathrm{i}\phi_{H_j})$, $j = 1, 2, 3$ into Eqs. (17a)–(17c), the existence of real physical solutions requires

$$\phi/2 + \phi_{H_2} - \phi_{H_1} - \phi_{H_3} = 0, \pi. \tag{19}$$

Two positive solutions are found given by

$$\alpha_{H_\pm} = \frac{\pm|\Gamma_4| - \sqrt{\Gamma_4^2 - 32\epsilon^2(\Gamma_2 + 2\Gamma_5)}}{4\epsilon(\Gamma_2 + 2\Gamma_5)}. \tag{20}$$

Also solutions with $\alpha_H < 0$ exist which would correspond to negative hexagons but they are not found numerically and anticipated to be unstable.

By expanding the original amplitude to order ϵ, we obtain $A = A_0 + B \approx A_t + \epsilon B^{(1)}$ which leads to

$$A_R = A_t + 2\epsilon e^{i\phi/2}\alpha_R \cos k_c x, \tag{21a}$$

$$A_S = A_t + 2\epsilon e^{i\phi/2}\alpha_S[\cos k_c x + \cos k_c y], \tag{21b}$$

$$A_{H_\pm} = A_t + 2\epsilon e^{i\phi/2}\alpha_{H_\pm}[\cos k_c x_1 + \cos k_c x_2 + \cos k_c x_3]. \tag{21c}$$

Hence, the patterns consist of a spatially modulated part on a homogeneous background. The peak intensities of the rolls, squares and hexagons are given by

$$|A_R^{\max}|^2 = |A_t|^2 + 4\epsilon\alpha_R|A_t||\cos(\phi_A - \phi/2)|, \tag{22a}$$

$$|A_S^{\max}|^2 = |A_t|^2 + 8\epsilon\alpha_S|A_t||\cos(\phi_A - \phi/2)|, \tag{22b}$$

$$|A_{H_\pm}^{\max}|^2 = |A_t|^2 + 12\epsilon\alpha_{H_\pm}|A_t||\cos(\phi_A - \phi/2)|, \tag{22c}$$

where ϕ_A is the phase of A_t.

As discussed in the next section roll patterns do not appear spontaneously in the 2D configuration. However, in 1D configurations, that experimentally can be realized by implementing a nonlinear waveguide, they are expected to be common. The results from the amplitude equation can be compared directly to 1D numerics. An example is given in Fig. 3 that shows the roll amplitude variation when increasing the pump amplitude above instability threshold for one choice of system parameters $\Delta = -1.5$, $\xi = 4.5$. We observe exact agreement between numerics and the analytical solution close to threshold while further above threshold the analytical solution starts to deviate from the numerics. This is as expected since the multiple-scale analysis relies on a perturbative expansion valid only close to the instability threshold.

Squares and hexagons appear spontaneously in the system. For negative fundamental detuning the amplitude equations for squares can be shown not to have any physically relevant solutions which means squares do not exist, and instead the dynamics is dominated by hexagons. For positive detuning of the fundamental both square and hexagon branches exist as demonstrated in Ref. [15].

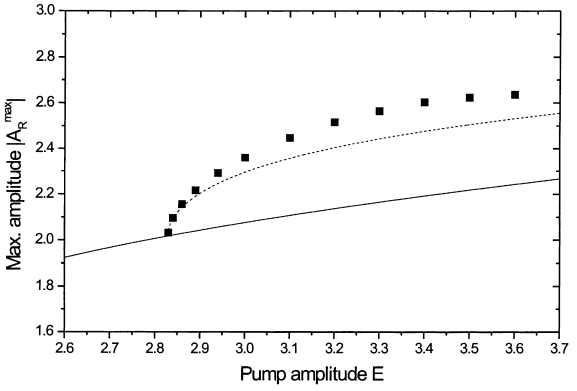

Fig. 3. Comparison between numerical (■) and analytical (- - -) solutions for 1D rolls. The plotted quantity is the roll pattern amplitude $|A_R^{\max}|$ as a function of the pump amplitude E. The full curve is the homogeneous solution that destabilize at the instability threshold. The detuning is $\Delta = -1.5$ and phase-mismatch $\xi = 4.5$.

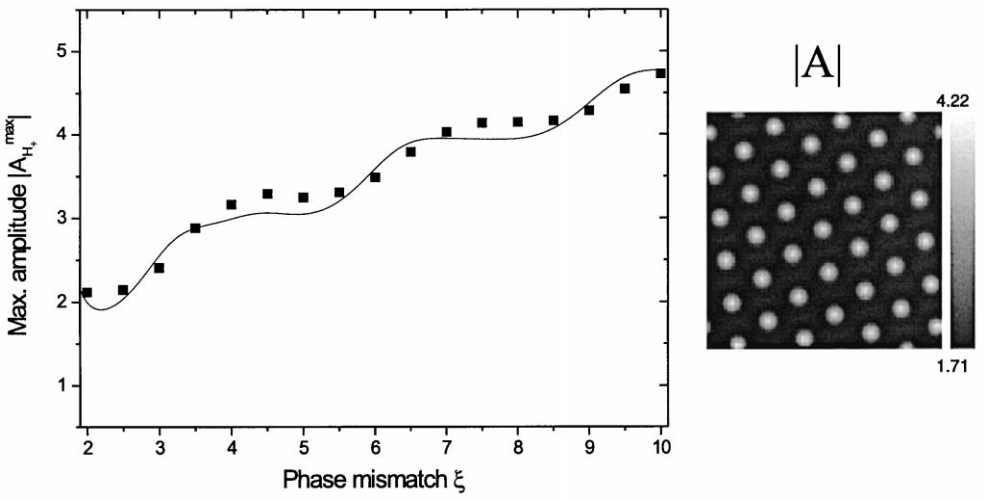

Fig. 4. Amplitude of the H_+ hexagons as a function of the phase-mismatch parameter ξ for $\Delta = 0$ and $\epsilon = 0.2$. The curve shows the analytical results from the amplitude equations while the points are from numerical simulations.

The hexagons can bifurcate subcritically which is generic for systems without inversion symmetry, and is described by the quadratic terms in the hexagon amplitude equations [26]. Note that the solution $A_{H_+}(\epsilon = 0) - A_t = 0$, while $A_{H_-}(\epsilon = 0) - A_t > 0$. Thus A_{H_+} is a supercritical hexagon branch and A_{H_-} represents the subcritical branch. However, as mentioned previously the subcritical region cannot be described by our analysis due to the choice of ϵ. Therefore in the following we will only look above threshold where $\epsilon^2 > 0$. In order to test the predictions of the hexagon amplitude equations, a detailed comparison with numerics is performed. As discussed above, two branches of hexagons H_+ and H_- exist, and both can be excited in the system depending on the detuning. Fig. 4 displays the hexagon amplitudes obtained from numerics together with the amplitude equation results for H_+ hexagons at resonance ($\Delta = 0$), and plotted as a function of the phase-mismatch parameter ξ. In this plot the pump level E is varied with the parameters in order to keep the expansion parameter fixed at $\epsilon = 0.2$. Rather convincing agreement is observed, thus establishing the applicability of the amplitude equations in the resonant case. In this resonant case the supercritical H_- branch was not found numerically.

As mentioned previously, a purely dispersive Kerr type nonlinearity is obtained for $\xi = m\pi$ with m an integer. Hence, it is of interest to consider this special case to check our results against previous work. For $\xi = \pi$ which corresponds to a self-focusing nonlinearity we find that the coefficient Γ_2 is positive for $\Delta < -41/30$ and becomes negative for $\Delta > -41/30$. Looking at Eq. (18a) we see that this implies that the supercritical roll bifurcation exists for $\Delta > -41/30$, in agreement with the well-known result for a Kerr cavity [18]. In the self-defocusing case ($\xi = -\pi$) we find $\Gamma_2 > 0$ so that the supercritical roll bifurcation does not exist. Thus, even though the present analysis cannot be used in the subcritical region, it predicts correctly the transition from subcritical to supercritical bifurcations in one transverse dimension.

For hexagons, we will restrict to the case of a self-focusing nonlinearity. Fig. 5 shows the hexagon amplitudes plotted as a function of the fundamental detuning for $\xi = \pi$ (other positive values of m are equivalent by rescaling of Eq. (1)) and with $\epsilon = 0.2$. The analytical results for both the H_+ and H_- hexagon branches are shown in addition to the numerical results. For positive detuning both hexagon branches are found numerically and while the H_+ hexagons agree well with the analytical results at small detuning and deviate gradually with increasing Δ, the opposite is true for the H_- hexagons. Such a deviation between analytics and numerics for H_+ hexagons with increased pump detuning was previously reported in the Kerr

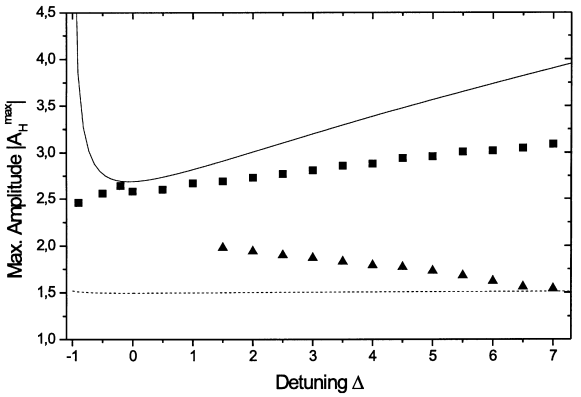

Fig. 5. Analytical results for the amplitude of H_+ (—) and H_- (- - -) hexagons as a function of the fundamental detuning Δ. The phase-mismatch parameter is $\xi = \pi$ corresponding to a Kerr type nonlinearity and the expansion parameter is $\epsilon = 0.2$. The corresponding numerical results are H_+ (■) and H_- (▲) hexagons respectively.

system [22]. For negative detuning only a branch of H_+ hexagons is found although the increase in pattern amplitude expected when decreasing the detuning towards the boundary of existence of the transverse instability is not found. In general the hexagons in this region were observed to suffer from defects which might explain the lack of agreement with the amplitude equation result. The H_+ hexagons were previously studied in Ref. [23] although only for the case of negative detuning (according to our sign convention) which might explain the fact that H_- hexagons were not found numerically.

3.2. Stability of patterns

The amplitude equations can be used to investigate analytically the stability of patterns. Here we will restrict to the most simple case of rolls and show that they cannot exist in the 2D configuration which is in agreement with the numerical observations. The stability of the roll solution is tested by perturbing according to $\alpha_1 = \alpha_R + \delta\alpha_1^{(+)}e^{\lambda_1 t + i\mathbf{k}_1\cdot\mathbf{r}} + \delta\alpha_1^{(-)}e^{\lambda_1^* t - i\mathbf{k}_1\cdot\mathbf{r}}$, $\alpha_2 = \delta\alpha_2^{(+)}e^{\lambda_2 t + i\mathbf{k}_2\cdot\mathbf{r}} + \delta\alpha_2^{(-)}e^{\lambda_2^* t - i\mathbf{k}_2\cdot\mathbf{r}}$, and substituting into Eqs. (16a) and (16b). Using Eq. (18a), we obtain the equations

$$\begin{bmatrix} \lambda_1 + 2\epsilon^2 + \Gamma_1 Q_{+,1}^2 & 2\epsilon^2 \\ 2\epsilon^2 & \lambda_1 + 2\epsilon^2 + \Gamma_1 Q_{-,1}^2 \end{bmatrix} \begin{pmatrix} \delta\alpha_1^{(+)} \\ \left(\delta\alpha_1^{(-)}\right)^* \end{pmatrix} = \begin{pmatrix} 0 \\ 0 \end{pmatrix}, \tag{23a}$$

$$\begin{bmatrix} \lambda_2^{(+)} - 2\epsilon^2(1 - \Gamma_3/\Gamma_2) + \Gamma_1 Q_{+,2}^2 & 0 \\ 0 & \lambda_2^{(-)} - 2\epsilon^2(1 - \Gamma_3/\Gamma_2) + \Gamma_1 Q_{-,2}^2 \end{bmatrix} \begin{pmatrix} \delta\alpha_2^{(+)} \\ \left(\delta\alpha_2^{(-)}\right)^* \end{pmatrix} = \begin{pmatrix} 0 \\ 0 \end{pmatrix}, \tag{23b}$$

with $Q_{\pm,j} = k_{y,j}^2 \pm 2k_c k_{x,j}$. The solutions are

$$\lambda_1^{(\pm)} = -2\epsilon^2 - \tfrac{1}{2}\Gamma_1\left(Q_{+,1}^2 + Q_{-,1}^2\right) \pm \tfrac{1}{2}\sqrt{16\epsilon^4 + \Gamma_1^2\left(Q_{+,1}^2 - Q_{-,1}^2\right)^2}, \tag{24a}$$

$$\lambda_2^{(\pm)} = 2\epsilon^2(1 - \Gamma_3/\Gamma_2) - \Gamma_1 Q_{\pm,2}. \tag{24b}$$

It is easily shown that $\lambda_1^{(\pm)} \leqslant 0$, while $\lambda_2^{(\pm)}$ can become positive leading to oscillation of the amplitude α_2 and thus to destabilization of the roll pattern. We note that the largest eigenvalue λ_{max} is obtained when $Q_{\pm,2} = 0$.

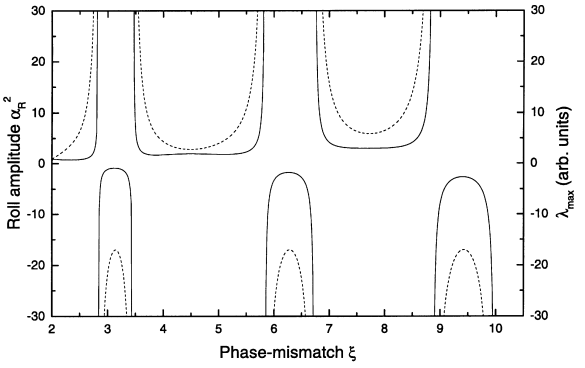

Fig. 6. Roll amplitude α_R^2 (—) and largest eigenvalue λ_{max} (- - -) as a function of the phase-mismatch parameter ξ. The fundamental detuning is $\Delta = -1.5$.

Two conditions need to be fulfilled to obtain roll patterns spontaneously in the system; $\alpha_R^2 > 0$ is required for the solution to exist and $\lambda_{max} < 0$ for it to be stable. It does not seem to be possible to satisfy both requirements simultaneously in the 2D configuration. For positive detuning $\Delta > 0$ the roll patterns are found to be unstable. The negative detuning case $\Delta < 0$ is slightly more complicated since parameters exist where λ_{max} becomes negative. However, this only occurs when $\alpha_R^2 < 0$ and consequently the roll solution does not exist. An example is given in Fig. 6 where the square of the roll amplitude and the maximal eigenvalue are plotted as a function of the phase-mismatch parameter in the case of $\Delta = -1.5$. The absence of roll patterns presented here is in contrast to the dominating role they play in the OPO [3–5] and in non-degenerate SHG [12–14].

4. Conclusions

We have investigated transverse pattern formation in SRSHG. Starting from a mean-field cavity equation for the fundamental field, amplitude equations describing the pattern formation dynamics above instability threshold were derived through a multiple-scales analysis. These generic amplitude equations describe roll, square and hexagonal patterns. A detailed comparison between the predictions of the amplitude equations and the numerical solution of the original mean-field equation showed good agreement extending well above threshold and in large parameter regions. This constitutes the validity of the approximate amplitude equations and is furthermore a good test of the numerics. Finally, the amplitude equations were used to show that roll patterns are always unstable with respect to square patterns, thus explaining their lack of appearance in the numerical simulations.

Acknowledgements

P.L. acknowledges support from the Danish Research Academy.

Appendix A. Derivation of amplitude equations

This appendix gives some mathematical details in the derivation of the amplitude equations. We will restrict to the case of atmost two critical wave vector components corresponding to rolls and squares.

To order ϵ^2, Eq. (13b) must be solved. This is a linear differential equation for $\mathbf{v}^{(2)}$ and the Fredholm solvability criterion [2] can be used to obtain equations for the undetermined amplitudes in $\mathbf{v}^{(1)}$. For that purpose vectors in the kernel of $\hat{\mathbf{L}}_0^{\dagger}$ must be found and convenient choices are $\mathbf{u}_j = (\mathrm{e}^{\mathrm{i}\phi}, 1)^{\mathrm{T}}\mathrm{e}^{\mathrm{i}k_c x_j}$, $j = 1, 2$. The solvability criterion is expressed as the inner product $\langle \mathbf{u}_j, \hat{\mathbf{L}}_1\mathbf{v}^{(1)} - \partial_{T_1}\mathbf{v}^{(1)} + \mathbf{N}_2\rangle = 0$. Evaluating the expressions leads to

$$\partial_{T_1}\alpha_j = 0, \quad j = 1, 2. \tag{A.1}$$

To solve Eq. (13b) we substitute a solution of the form

$$\begin{aligned} B^{(2)} = {} & 2\beta + \gamma_1\mathrm{e}^{\mathrm{i}k_c x_1} + \gamma_2\mathrm{e}^{-\mathrm{i}k_c x_1} + \gamma_3\mathrm{e}^{\mathrm{i}k_c x_2} + \gamma_4\mathrm{e}^{-\mathrm{i}k_c x_2} + \delta_1\mathrm{e}^{\mathrm{i}\phi}\mathrm{e}^{2\mathrm{i}k_c x_1} + \delta_2\mathrm{e}^{-\mathrm{i}\phi}\mathrm{e}^{-2\mathrm{i}k_c x_1} + \delta_3\mathrm{e}^{\mathrm{i}\phi}\mathrm{e}^{2\mathrm{i}k_c x_2} \\ & + \delta_4\mathrm{e}^{-\mathrm{i}\phi}\mathrm{e}^{-2\mathrm{i}k_c x_2} + 2\eta_1\mathrm{e}^{\mathrm{i}\phi}\mathrm{e}^{\mathrm{i}k_c(x_1+x_2)} + 2\eta_2\mathrm{e}^{-\mathrm{i}\phi}\mathrm{e}^{-\mathrm{i}k_c(x_1+x_2)} + 2\eta_3\mathrm{e}^{\mathrm{i}k_c(x_1-x_2)} + 2\eta_4\mathrm{e}^{-\mathrm{i}k_c(x_1-x_2)}. \end{aligned} \tag{A.2}$$

Inserting into Eq. (13b) leads to the following set of equations

$$\hat{\mathbf{M}}\begin{pmatrix} \beta \\ \beta^* \end{pmatrix} = \left(|\alpha_1|^2 + |\alpha_2|^2\right)\mathbf{w}, \tag{A.3a}$$

$$\left(\hat{\mathbf{M}} + \hat{\mathbf{J}}\right)\begin{pmatrix} \gamma_{2j-1} \\ \gamma_{2j}^* \end{pmatrix} = \begin{pmatrix} \mathrm{i}\partial_{Y_j}^2 - 2k_c\partial_{X_j} - \partial_{T_1} \\ \mathrm{e}^{-\mathrm{i}\phi}\left[-\mathrm{i}\partial_{Y_j}^2 + 2k_c\partial_{X_j} - \partial_{T_1}\right] \end{pmatrix}\alpha_j, \tag{A.3b}$$

$$\left(\hat{\mathbf{M}} + 4\hat{\mathbf{J}}\right)\begin{pmatrix} \delta_{2j-1} \\ \delta_{2j}^* \end{pmatrix} = \alpha_j^2\mathbf{w}, \tag{A.3c}$$

$$\left(\hat{\mathbf{M}} + 2[1+\cos\theta]\hat{\mathbf{J}}\right)\begin{pmatrix} \eta_1 \\ \eta_2^* \end{pmatrix} = \alpha_1\alpha_2\mathbf{w}, \tag{A.3d}$$

$$\left(\hat{\mathbf{M}} + 2[1-\cos\theta]\hat{\mathbf{J}}\right)\begin{pmatrix} \eta_3 \\ \eta_4^* \end{pmatrix} = \alpha_1\alpha_2^*\mathbf{w}, \tag{A.3e}$$

with $j = 1, 2$, $\theta = \theta_{12}$, and

$$\hat{\mathbf{M}} = \begin{bmatrix} 1 - \mathrm{i}\Delta - 2f|A_t|^2 & -fA_t^2 \\ -f^*A_t^{*2} & 1 + \mathrm{i}\Delta - 2f^*|A_t|^2 \end{bmatrix}, \tag{A.4a}$$

$$\hat{\mathbf{J}} = \begin{bmatrix} \mathrm{i}k_c^2 & 0 \\ 0 & -\mathrm{i}k_c^2 \end{bmatrix}, \tag{A.4b}$$

$$\mathbf{w} = \begin{pmatrix} f\left(2A_t + A_t^*\mathrm{e}^{\mathrm{i}\phi}\right) \\ f^*\left(2A_t^* + A_t\mathrm{e}^{-\mathrm{i}\phi}\right) \end{pmatrix}. \tag{A.4c}$$

The equations can be solved by using Eqs. (4), (15) and (A.1)

$$\beta = \tilde{\beta}\left(|\alpha_1|^2 + |\alpha_2|^2\right), \tag{A.5a}$$

$$\gamma_{2j-1} - \mathrm{e}^{\mathrm{i}\phi}\gamma_{2j}^* = \frac{\left(\mathrm{i}\partial_{Y_j}^2 - 2k_c\partial_{X_j}\right)\alpha_j}{1 - 2f_r|A_t|^2}, \tag{A.5b}$$

$$\delta_{2j-1} = \tilde{\delta}\alpha_j^2, \tag{A.5c}$$

$$\delta_{2j}^* = \tilde{\delta}^*\alpha_j^2, \tag{A.5d}$$

$$\eta_1 = \tilde{\eta}_+ \alpha_1 \alpha_2, \tag{A.5e}$$

$$\eta_2^* = \tilde{\eta}_+^* \alpha_1 \alpha_2, \tag{A.5f}$$

$$\eta_3 = \tilde{\eta}_- \alpha_1 \alpha_2^*, \tag{A.5g}$$

$$\eta_4^* = \tilde{\eta}_-^* \alpha_1 \alpha_2^*, \tag{A.5h}$$

where the coefficients are

$$\tilde{\beta} = \frac{(1 - 2f_r|A_t|^2)(w + w^* e^{i\phi}) + ik_c^2 w}{k_c^4}, \tag{A.6a}$$

$$\tilde{\delta} = \frac{(1 - 2f_r|A_t|^2)(w + w^* e^{i\phi}) - 3ik_c^2 w}{9k_c^4}, \tag{A.6b}$$

$$\tilde{\eta}_\pm(\theta) = \frac{(1 - 2f_r|A_t|^2)(w + w^* e^{i\phi}) - ik_c^2(1 \pm 2\cos\theta)w}{(1 \pm 2\cos\theta)^2 k_c^4}, \tag{A.6c}$$

and w is the first component of the vector in Eq. (A.4c).

Eq. (13c) is the third-order contribution in the perturbation expansion. Evaluating the solvability criterion $\langle \mathbf{u}_j, \hat{\mathbf{L}}_2 \mathbf{v}^{(1)} - \partial_{T_2} \mathbf{v}^{(1)} + \hat{\mathbf{L}}_1 \mathbf{v}^{(2)} - \partial_{T_1} \mathbf{v}^{(2)} + \mathbf{N}_3 \rangle = 0$ and using the second-order solution in Eq. (A.2), two coupled equations are obtained

$$\partial_{T_2} \alpha_1 = \Gamma_1 \left(i\partial_{Y_1}^2 - 2k_c \partial_{X_1} \right)^2 \alpha_1 + 2\alpha_1 + \left(\Gamma_2 |\alpha_1|^2 + \Gamma_3 |\alpha_2|^2 \right) \alpha_1, \tag{A.7a}$$

$$\partial_{T_2} \alpha_2 = \Gamma_1 \left(i\partial_{Y_2}^2 - 2k_c \partial_{X_2} \right)^2 \alpha_2 + 2\alpha_2 + \left(\Gamma_2 |\alpha_2|^2 + \Gamma_3 |\alpha_1|^2 \right) \alpha_2, \tag{A.7b}$$

where

$$\Gamma_1 = \frac{1}{2(1 - 2f_r|A_t|^2)}, \tag{A.8a}$$

$$\Gamma_2 = \left[2fA_t \left(2\tilde{\beta}^* + 2\tilde{\beta} e^{-i\phi} + \tilde{\delta}^* + \tilde{\delta} e^{-i\phi} \right) \right]_r + \left[2fA_t^* \left(2\tilde{\beta} + \tilde{\delta} \right) \right]_r + 3f_r, \tag{A.8b}$$

$$\Gamma_3(\theta_{12}) = \left[4fA_t \left(\tilde{\beta}^* + \tilde{\beta} e^{-i\phi} + \tilde{\eta}_-^* + \tilde{\eta}_- e^{-i\phi} + \tilde{\eta}_+^* + \tilde{\eta}_+ e^{-i\phi} \right) \right]_r + \left[4fA_t^* \left(\tilde{\beta} + \tilde{\eta}_+ + \tilde{\eta}_- \right) \right]_r + 6f_r. \tag{A.8c}$$

Finally reintroducing the original space and time variables in Eqs. (A.7a) and (A.7b) leads to the amplitude equations (16a) and (16b) for rolls and squares. A similar analysis can be performed for hexagons. This leads to the introduction of the following coefficients

$$\Gamma_4 = \left[8fA_t e^{-i\phi/2} \right]_r + \left[4fA_t^* e^{i\phi/2} \right]_r, \tag{A.9}$$

$$\Gamma_5 = \left[4fA_t \left(\tilde{\beta}^* + \tilde{\beta} e^{-i\phi} + \tilde{\eta}_+^*(\pi/3) + \tilde{\eta}_+(\pi/3) e^{-i\phi} \right) \right]_r + \left[4fA_t^* \left(\tilde{\beta} + \tilde{\eta}_+(\pi/3) \right) \right]_r + 6f_r, \tag{A.10}$$

that appear in Eqs. (17a)–(17c).

References

[1] M.C. Cross, P.C. Hohenberg, Rev. Mod. Phys. 65 (1993) 851.
[2] P. Manneville, Dissipative Structures and Weak Turbulence, Academic Press, New York, 1990.

[3] G.-L. Oppo, M. Brambilla, L.A. Lugiato, Phys. Rev. A 49 (1994) 2028.
[4] G.-L. Oppo, M. Brambilla, D. Camesasca, A. Gatti, L.A. Lugiato, J. Mod. Opt. 41 (1994) 1151.
[5] G.J. de Valcárcel, K. Staliunas, E. Roldán, V.J. Sánchez-Morcillo, Phys. Rev. A 54 (1996) 1609.
[6] S. Longhi, Phys. Rev. A 53 (1996) 4488.
[7] P.K. Jakobsen, J.V. Moloney, A.C. Newell, R. Indik, Phys. Rev. A 45 (1992) 8129.
[8] P.K. Jakobsen, J. Lega, Q. Feng, M. Staley, J.V. Moloney, A.C. Newell, Phys. Rev. A 49 (1994) 4189.
[9] J. Lega, P.K. Jakobsen, J.V. Moloney, A.C. Newell, Phys. Rev. A 49 (1994) 4201.
[10] C. Etrich, U. Peschel, F. Lederer, Phys. Rev. E 56 (1997) 4803.
[11] S. Longhi, Opt. Lett. 23 (1998) 346.
[12] C. Etrich, D. Michaelis, U. Peschel, F. Lederer, Phys. Rev. E 58 (1998) 4005.
[13] S. Longhi, Phys. Rev. E 59 (1999) R24.
[14] S. Longhi, Phys. Rev. A 59 (1999) 4021.
[15] P. Lodahl, M. Saffman, Phys. Rev. A 60 (1999) 3251.
[16] M.A.M. Marte, Phys. Rev. A 49 (1994) R3166.
[17] P. Lodahl, M. Bache, M. Saffman, Opt. Lett. 25 (2000) 654.
[18] L.A. Lugiato, R. Lefever, Phys. Rev. Lett. 58 (1987) 2209.
[19] L.A. Lugiato, C. Oldano, Phys. Rev. A 37 (1988) 3896.
[20] L.A. Lugiato, W. Kaige, N.B. Abraham, Phys. Rev. A 49 (1994) 2049.
[21] M. Tlidi, M. Georgiou, P. Mandel, Phys. Rev. A 48 (1993) 4605.
[22] A.J. Scroggie, W.J. Firth, G.S. McDonald, M. Tlidi, R. Lefever, L.A. Lugiato, Chaos, Solitons & Fractals 4 (1994) 1323.
[23] M. Tlidi, R. Lefever, P. Mandel, Quant. Semiclass. Opt. 8 (1996) 931.
[24] A.C. Newell, J.A. Whitehead, J. Fluid Mech. 38 (1969) 279.
[25] L.A. Segel, in: R.J. Donnelly, R. Herman, I. Prigogine (Eds.), Non-equilibrium Thermodynamics, Variational Techniques and Stability, University of Chicago Press, 1966.
[26] S. Ciliberto, P. Coullet, J. Lega, E. Pampaloni, C. Perez-Garcia, Phys. Rev. Lett. 65 (1990) 2370.